



## Dynamic nanostructures at the surface of rising bubbles in amphiphile solutions: Comparison of low-molecular-weight surfactants and proteins

Ł. Witkowski<sup>a</sup>, A. Wiertel-Pochopien<sup>a</sup>, D. Kosior<sup>a</sup>, G. Gochev<sup>a,b</sup>, P. Warszynski<sup>a</sup>, G.G. Fuller<sup>c</sup>, J. Zawala<sup>a,\*</sup>

<sup>a</sup> Jerzy Haber Institute of Catalysis and Surface Chemistry, Polish Academy of Sciences, 30239 Krakow, Poland

<sup>b</sup> Institute of Physical Chemistry, Bulgarian Academy of Sciences, 1113 Sofia, Bulgaria

<sup>c</sup> Department of Chemical Engineering, Stanford University, Stanford, CA 94305, USA

### ARTICLE INFO

#### Keywords:

Bubble  
Dynamic adsorption layer  
Surfactant  
Macromolecule  
Velocity

### ABSTRACT

The formation, stability, and decay of foams occur under dynamic conditions. Given their inherent complexity, an accurate description of these subprocesses necessitates an analysis of multiple factors, with a particular focus on the formation and structure of the adsorption layer. Single rising bubble techniques facilitate a deeper comprehension of the dynamics of diverse phenomena in foams, as they yield experimental data under dynamic conditions. This review examines the subtle differences in the dynamic adsorption structures of low-molecular-weight surfactants and proteins at the liquid/gas interface. These differences can significantly impact interfacial properties and potentially alter our understanding of the mechanisms behind the formation of the Dynamic Adsorption Layer (DAL). The primary techniques under consideration are local velocity profiles (LVPs) of single rising bubbles and dynamic fluid-film interferometry (DFI) of the thin liquid film formed at the collision of a bubble with a free liquid surface. We provide a summary of recent findings on the topic. Due to the limited availability of comprehensive datasets on proteins, our discussion is partially supplemented by newly obtained unpublished data. We highlight key differences in the behavior of bubbles in low-molecular-weight surfactant solutions versus protein solutions that have previously been overlooked in the literature. We explore their potential origins in the context of DAL dynamics and architecture.

### 1. Introduction

Understanding the formation, stability, and decay of foams is essential across various industries, including mineral processing [1,2], food production [3], firefighting [4], cleansing agents [5], and cosmetic and pharmaceutical applications [6,7]. Foams are stabilized by surface-active agents, primarily surfactants, which reduce surface tension and promote the formation of stable bubbles. However, many synthetic surfactants degrade slowly and pose potential environmental risks [8]. In response, research has increasingly focused on biodegradable and environmentally benign alternatives [9,10], with proteins emerging as one of the most promising candidates for stabilizing foams and emulsions [11,12]. Protein-based foaming agents are particularly relevant in the food industry, where their natural origin and biocompatibility are advantageous [3,13]. Proteins possess intrinsic surface activity, making them well-suited for foam-based separation techniques such as foam fractionation [14–17] and colloidal gas apheresis [18–22]. Foam

fractionation, first developed in the 1960s [23,24], has since found applications in diverse areas, including water treatment [25,26] and product concentration during downstream processing [27,28]. However, its primary role remains in protein purification and enrichment [29–31]. The stability of foams is governed by interfacial phenomena at liquid/gas boundaries, where adsorption processes influence the formation and mechanical properties of interfacial films. A comprehensive understanding of these adsorption dynamics is crucial for optimizing foam performance in industrial settings [32].

Several experimental techniques are employed for probing soft interfaces and to investigate adsorption at liquid/gas interfaces [33]. Traditional methods include surface tension measurements and surface excess determination [34–36], as well as rheological assessments of interfacial shear and dilatational properties [32,37]. More advanced experimental approaches, such as microscopy [38], spectroscopy [39,40] and reflectometry [33], have provided new insights into adsorption kinetics and interfacial structuring. Additionally, studies on

\* Corresponding author.

E-mail address: [jan.zawala@ikifp.edu.pl](mailto:jan.zawala@ikifp.edu.pl) (J. Zawala).

<https://doi.org/10.1016/j.cis.2025.103447>

Received in revised form 16 February 2025;

Available online 27 February 2025

0001-8686/© 2025 The Authors. Published by Elsevier B.V. This is an open access article under the CC BY license (<http://creativecommons.org/licenses/by/4.0/>).

thin liquid films (TLFs) [32,33,41,42] help connect single-interface properties to macroscopic foam behavior. TLF research has primarily focused on quasi-static conditions, leaving dynamic processes such as foam formation and decay less understood. The investigations, complemented by modelling of experimental data [43,44] and together with molecular dynamics simulations [45], provide accurate information about fundamental, optical, mechanical and structural properties of interfacial layers and surface forces in TLFs [32] and the process of coalescence [46]. Addressing existing gaps is critical for improving foam-related technologies and industrial applications [47].

Bubble formation and movement play a key role in foam dynamics, influencing stability and longevity [48,49]. This is particularly relevant in three-phase systems, such as flotation aggregates, where gas bubbles facilitate the separation of dispersed particles [50,51]. The motion of rising bubbles is significantly affected by the presence of surfactants, which form dynamic adsorption layer (DAL) at the bubble interface [52–56]. The literature on DAL formation at the surface of a single bubble rising in a surfactant solution is extensive. It ranges from experimental studies aimed at determining the kinetics of DAL formation [50,51,54,57–62] to theoretical works that quantify this phenomenon in terms of characteristic parameters that are sensitive to the hydrodynamic and physicochemical conditions under which the bubble motion proceeds [53,55,56,63–65]. It is accepted that DAL formation alters interfacial properties, leading to variations in drag and changes in bubble hydrodynamics. The redistribution of surfactant molecules along the bubble's surface creates surface convection patterns and generates surface tension gradients [56], ultimately influencing the bubble's rise velocity and stability.

Bubble motion in solution of surface-active species typically progresses through four distinct stages: acceleration, peak velocity, deceleration, and terminal velocity ( $u_t$ ), which can be revealed by determination of a bubble velocity profiles (LVPs). These stages are influenced by surfactant concentration, solvent conditions (such as pH and electrolyte composition), and the physicochemical properties of the surfactant [66]. The stagnant cap theory is commonly used to describe bubble dynamics in surfactant-laden solutions [53,56,63]. According to this model, the bubble interface contains both mobile and immobilized regions, with surfactant molecules accumulating at the rear of the rising bubble to form a stagnant zone (see Fig. 1A). This uneven distribution of surfactant results in characteristic surface tension gradients that influence bubble motion. While analytical models exist to describe terminal bubble velocity under steady-state conditions, capturing the full complexity of DAL evolution remains challenging. The interplay between surfactant adsorption, desorption, and surface tension gradients adds to the difficulty of developing a comprehensive framework that accounts for bubble hydrodynamics across a wide range of Reynolds numbers and physicochemical environments. This is why, despite numerous studies, a fully predictive theoretical model that describes bubble motion under varying flow and interfacial conditions remains elusive.

Computational fluid dynamics (CFD) represents a promising methodology for future investigations of DAL kinetics. By simulating the

interactions between surfactant molecules, flow fields, and interfacial forces, CFD allows for a detailed examination of how bubble dynamics evolve under various conditions. Several studies have successfully modeled surfactant adsorption and transport, revealing intricate velocity profiles and interfacial stress distributions. For example, Tukovic and Jasak [67,68], followed by Pesci et al. [69], developed models based on two-fluid systems with a sharp interface and soluble surfactants. Using the Finite Volume Method, they tracked bubble motion and interfacial deformations, solving the Navier-Stokes equations to describe mass and momentum conservation. Their approach linked surface tension to surfactant concentration via the Frumkin-Langmuir equation of state, offering insights into dynamic changes in surface coverage. These simulations gave direct insights into the velocities and flow lines of the surrounding liquid (see Fig. 1B,C) and dynamic changes in the surface concentration of surfactants, as well as demonstrated how different surfactant concentrations and bubble sizes lead to distinct bubble trajectories, such as zig-zag or helical paths. More recently, Wang et al. [70] developed a model where a spherical bubble of fixed radius was analyzed within a surfactant solution, providing angular dependencies of near-surface velocity and shear forces. Such computational models contribute to a deeper understanding of bubble-surfactant interactions, complementing experimental studies and advancing theoretical descriptions of DAL formation.

The state-of-the-art literature provides extensive experimental data on the impact of surface-active substances with varying surface activities and diffusion characteristics on DAL formation rates and kinetics. Our goal, therefore, is to highlight seemingly largely overlooked subtle differences in bubble dynamics in solutions of low-molecular-weight surfactants from one hand and, on the other hand, macromolecules (proteins, in particular). These differences have apparently significant implications on various interfacial properties and may alter our understanding of the mechanisms of adsorption and the architecture of DAL in macromolecular systems. Due to the acute lack of data on rising bubbles in protein solutions, we have utilized selected unpublished experimental data obtained through collaborative research efforts of the authors of this paper, which are referenced accordingly.

## 2. Experimental data on bubble velocity variations in aqueous solutions

### 2.1. Low-molecular-weight surfactants

The motion of a single bubble (with radius  $R$ ) in a liquid (with density  $\rho$  and dynamic viscosity  $\mu$ ) is typically analyzed in terms of two limiting cases: a fully mobile (slip) interface or a fully immobilized (no-slip) interface. In the first case, the liquid is free of any surface-active species [52,58,65,72], or the liquid/gas interface has very low free surface energy [73]. As a result, an “effective” adsorption layer is not formed, thus, the interface remains stress-free, leading to a minimal drag coefficient. Conversely, the adsorption of surface-active molecules can impede the mobility of the bubble's surface (either partially or fully), increasing the drag coefficient and reducing the bubble's rise velocity.

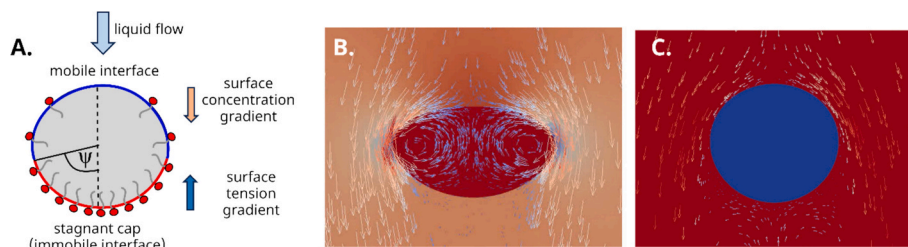


**Fig. 1.** Illustration of (A) dynamic adsorption layer at a single bubble rising in surfactant solution (scheme not to scale, compact zone, i.e. so-called “stagnant cap” is defined by the angle  $\psi$ ) and velocity fields around a rising bubble in (B) pure water and (C) high concentration of surfactant of relatively fast adsorption kinetics, reproduced based on the computational algorithm by Tukovic and Jasak [67,68] implemented into OpenFOAM [71].

For the first case (stress-free interface), Moore [74] theoretically described the drag coefficient and the resulting bubble terminal velocity  $u_t$  (the constant velocity under given hydrodynamic conditions), taking the bubble deformation into account:

$$C_D = \frac{48}{Re} G(\chi) \left[ 1 + \frac{H(\chi)}{\sqrt{Re}} + O\left(\frac{1}{\sqrt{Re}}\right) \right] \quad (1)$$

where  $Re$  is the Reynolds number ( $Re = 2Ru_t\rho_L/\mu$ );  $G(\chi)$  and  $H(\chi)$  are functions of a bubble deformation degree ( $\chi$ ), typically reported as:

$$\chi = d_h/d_v \quad (2)$$

with  $d_h$  and  $d_v$  being the horizontal and the vertical diameters of the bubble. These diameters can be used to calculate the so-called equivalent bubble diameter  $d_{eq} = (d_h^2 d_v)^{1/3}$ . The geometric parameters  $G(\chi)$  and  $H(\chi)$  for  $\chi < 2$  can be approximated by a second-order linear Eq. [75]. Predicting the  $\chi$ -value for a given bubble size requires an understanding of its relationship with the Weber number ( $We = 2Ru_t^2\rho/\sigma$ ), which can be approximated basing on the large number of experimental data reported in ref. [76] as:

$$\chi = \left( 1 - \frac{9}{64} We \right)^{-1} \quad (3)$$

Considering a dynamic equilibrium between buoyancy ( $F_B = 4/3\pi R^3\rho g$ ) and drag ( $F_D = 0.5\pi R^2 C_D \rho u_t^2$ ) forces for a bubble of radius  $R = 0.5d_{eq}$ , resulting in steady-state motion, the bubble terminal rise velocity can be expressed as:

$$u_t = \left( \frac{8Rg}{3C_D} \right)^{1/2} \quad (4)$$

where  $C_D$  is estimated from Eq. (1), which gives  $u_t$  for a bubble with fully mobile interface.

In the second limiting case, where a bubble interface fluidity is fully

retarded by DAL [65], the Schiller-Naumann equation, valid for  $Re < 800$ , is commonly used to calculate the drag coefficient of a bubble under steady-state motion [77]:

$$C_D = \frac{24}{Re} (1 + 0.15Re^{0.687}) \quad (5)$$

In practice, variations in the rising velocity of a single bubble are most commonly determined through video observations and image analysis of the captured bubble images. Although various precise experimental methods are available, such as ultrasound measurements [78], video recording remains the most frequently used and convenient tool for determining bubble motion parameters. These parameters include not only rising velocity but also variations in bubble size, shape, and trajectory [54,59,79]. Fig. 2 presents examples of experimentally determined bubble rising velocities (LVPs and  $u_t$ ) from the literature for different types of either nonionic or ionic low-molecular-weight surfactants [54,78]. As an example, the LVPs for solutions of n-octanol (a simple fatty alcohol) at different bulk concentrations are shown. In this case, the data were collected from three independent experiments, where bubble velocity calculations were performed frame-by-frame (i) manually by two individuals (using image analysis software) and (ii) an image analysis script written in Python. The  $u_t$  values presented in Fig. 2B were calculated from the sections of the velocity profiles where the local velocity was constant. The scenario depicted in Fig. 2 can be regarded as illustrative of the typical characteristics exhibited by low-molecular-weight surfactants. It demonstrates the prevailing trends and relationships between variations in bubble velocity with distance and surfactant solution concentration.

As discussed in a substantial body of literature [50,51,53,54,56,61,81–84], the characteristic shapes of LVPs during different stages of bubble motion – acceleration, maximum velocity, deceleration and constant velocity – can reveal information about the kinetics of DAL formation. The presence of a DAL immobilizes the liquid/gas interface, and notably, this effect proceeds in a gradual rather than an abrupt manner (see Fig. 2B). This implies that the hydrodynamic

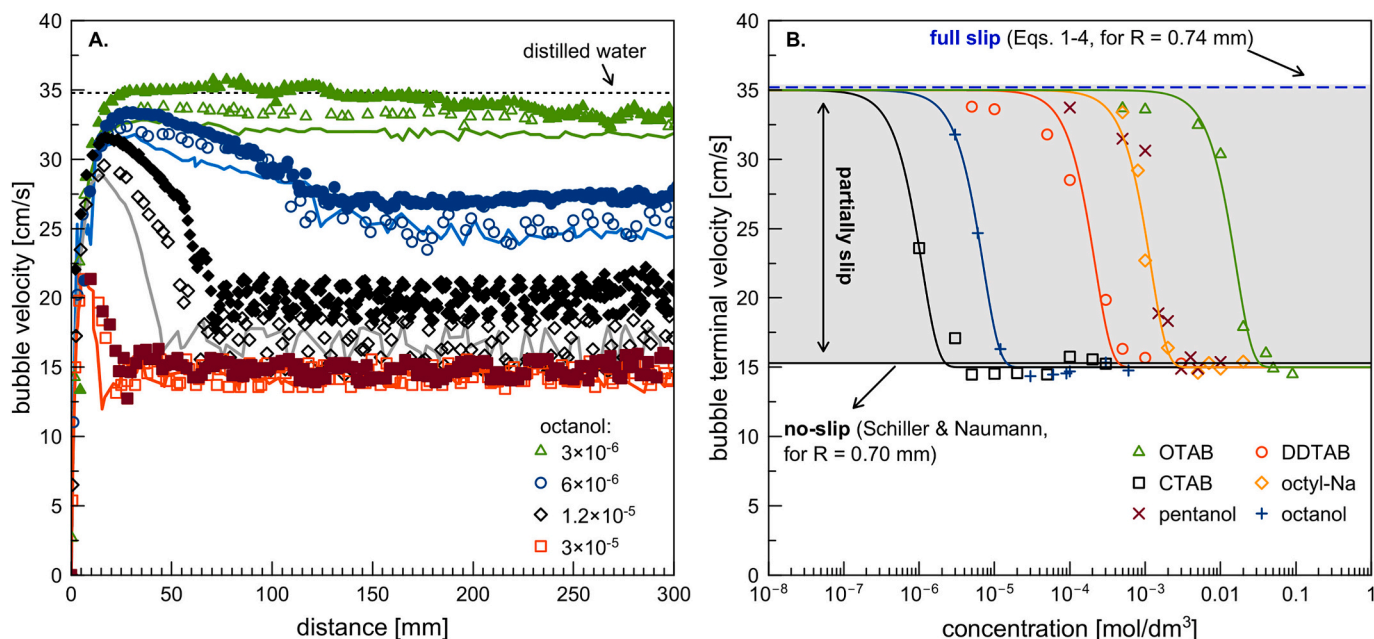


Fig. 2. (A) Experimental local velocity profiles (LVPs) of an air bubble ( $R_{eq} = 0.74$  mm) rising in n-octanol solutions in the pure water of different concentrations in  $[\text{mol}/\text{dm}^3]$  (hollow and full [54] symbols show results of manual image analysis performed by two different persons, lines denote results of analysis by Python script). (B) Bubble terminal velocity values for different types of low-molecular-weight surfactants (nonionic and ionic – symbols denote experimental data, lines are fits by Eq. (6) (with CMV as a fitting parameter); OTAB – octyl-trimethylammonium bromide [54], DDTAB – dodecyl-trimethylammonium bromide [54], CTAB – hexadecyl-trimethylammonium bromide [54], octyl-Na – sodium octyl sulfate – unpublished data, pentanol [80], octanol [54]). In Fig. 2B error bars were not included to maintain clarity in the picture.

boundary conditions at the surface of a rising bubble change from completely slip to partially slip or fully non-slip conditions, depending on the bulk concentration of the surfactant, which in turn, dictates the degree of liquid/gas interface immobilization and presumably determines the DAL's architecture. Kowalczyk et al. [85] recently proposed a convenient method for analyzing these effects and obtaining direct information about the limiting values of the surfactant concentration, which characterize complete immobilization of the bubble surface fluidity. A comprehensive dataset was collated from a number of laboratories, comprising solutions of various low-molecular-weight surfactants. This dataset was subjected to rigorous analysis, resulting in the derivation of a general empirical model:

$$u_t = u_{min} + (u_{max} - u_{min})e^{-3\left(\frac{c}{CMV}\right)^2} \quad (6)$$

where  $u_{min}$  and  $u_{max}$  are the minimum and maximum velocities of a rising bubble with a fully mobile and fully immobilized interface. The newly introduced characteristic parameter CMV (concentration at minimum velocity) is defined as the critical concentration at which the bubble velocity is minimized, i.e., the minimum surfactant bulk concentration required for complete immobilization of the bubble interface. The proposed equation can be used not only to compare this novel characteristic parameter (CMV) for different surfactants but also to predict the bubble terminal velocity as a function of surfactant concentration for partially immobilized interfaces, provided  $u_{min}$  and  $u_{max}$  are known (see the lines in Fig. 2B, which present results obtained using Eq. (6)).

## 2.2. Proteins

Proteins are complex biomacromolecules that play critical roles in living organisms. Furthermore, it is a well-known fact that proteins are extensively used in a great variety of processes and applications in medicine and traditional and modern technologies. Contrary to random-coil proteins (e.g. caseins and gelatins), which are, in fact, simple linear heteropolymers, globular proteins exhibit distinct secondary and tertiary structures, which determine their unique physicochemical and biological functionalities. From the perspective of the physical chemistry of interfaces, a protein can be viewed as a water-soluble macromolecular surfactant with a complex adsorption mechanism determined by various interrelated factors: from one hand, the nature of the interface (solid or fluid, and its degree of hydrophobicity) [45,86,87], and on the other hand, the intrinsic surface activity of a given protein, which in turn is strongly modulated by the solvent conditions (pH/electrolyte) [33,88].

Due to the inherent complexity of protein adsorption mechanisms and the challenges in describing these phenomena under static conditions, the literature on the influence of the protein concentration  $c_p$  on bubble motion is limited, with only a few studies addressing dynamic adsorption layer formation. However, these studies often treat proteins similarly to low-molecular-weight surfactants regarding the mechanisms responsible for bubble surface immobilization. Analysis of the available literature shows that bubble behavior, in terms of LVPs, is quite similar regardless of the type of protein used in the experiments [57,62,89–93] (bovine serum albumin - BSA [57,91],  $\beta$ -lactoglobulin [62,89,93], powdered egg white - EWP [90], or  $\beta$ -casein [89]). For example, LVPs obtained in BSA solutions (pH = 5.8) with  $c_p$  ranging from  $1.5 \times 10^{-8}$  to  $6 \times 10^{-7}$  mol/dm<sup>3</sup> are presented in Fig. 3A [91], resembling those shown in Fig. 2A. Similar stages of bubble motion can be distinguished in these profiles.

However, notable and intriguing features, which have never been mentioned before in the literature, have distinguished the behavior of a bubble in solutions of proteins from that of low-molecular-weight surfactants. As shown in Fig. 3A, regardless of the BSA solution concentration, the bubble velocities in the final stage of motion consistently

reach the lower velocity limit ( $u_{min} \approx 15$  cm/s) for the given bubble size ( $R = 0.73$  mm). This observation is, in fact, an important finding that reveals that a steady-state protein, DAL, is not fully capable of creating conditions that result in partial immobilization of the bubble interface. Furthermore, two distinct cases can be observed in the initial stages of bubble motion: for the lower BSA concentrations used, the maximum  $u$  in the LVPs virtually reaches the upper velocity limit for pure water ( $u_{max} \approx 35$  cm/s), while at the higher BSA concentrations used, the maximum  $u$  in the LVPs drops, which is indicative of partial immobilization of the liquid/gas interface. At a  $c_p = 4.5 \times 10^{-8}$  mol/dm<sup>3</sup>, the noticeable decrease in  $u$  did not result in the establishment of  $u_t$  due to experimental limitations – the LVP was incomplete because the liquid column was too short. Similar behavior has been reported in all studies involving various types of proteins. This effect is clearly illustrated in Fig. 3B, where  $u_t$  of bubbles of different sizes versus the solution concentration are compiled from various literature sources [57,62,90,91]. Full data point symbols represent  $u_t(R)$  values undoubtedly identified in experiments, while empty symbols indicate the last  $u$ -values recorded in incomplete LVPs (just before the end of the liquid column). As shown, no intermediate  $u$ -values (suggesting partial immobilization of the bubble surface) were reported, and the “true”  $u_t$  data reasonably follow the Schiller-Naumann model's predictions.

Another distinctive feature, unique to relatively high  $c_p$ , is a comparatively slight but noticeable increase in  $u$  after the deceleration stage has ended up at  $u_t$ . For low-molecular-weight surfactants, the establishment of  $u_t$  at  $u_{min}$  indicates that the DAL is fully formed, and as seen in Figs. 2, there are no further changes in  $u_t \approx u_{min}$  with distance (time). On the contrary, this phenomenon is observed for BSA concentrations of  $c_p = 4 \times 10^{-7}$  and  $c_p = 6 \times 10^{-7}$  mol/dm<sup>3</sup> (Fig. 3A) and it is depicted further in Fig. 4 for several proteins studied in the literature: 1) BSA ( $c_p = 4 \times 10^{-7}$  mol/dm<sup>3</sup>, pH 5.8) [91]; 2)  $\beta$ -lactoglobulin ( $c_p = 2 \times 10^{-6}$  mol/dm<sup>3</sup>, solution prepared in 10 mM citric/phosphate buffer at pH 7, and  $c_p = 5 \times 10^{-6}$  mol/dm<sup>3</sup>) [62,93]; and 3) egg white ( $c_p = 8.6 \times 10^{-7}$  mol/dm<sup>3</sup>) [90]. Apparently, the way  $u$  increases above  $u_{min}$  is virtually identical across all those results for the different protein types and  $c_p$ , with a distinct increase of approximately 2 cm/s, which is well above the typical standard deviation of about  $\pm 0.5$  cm/s. For example, for the BSA solution in Fig. 3A, the bubble velocity of  $u \approx 14.2$  cm/s (average value over the distance of 5–15 cm), which should be thought of as the value for  $u_t$ , gradually increases to 16.5 cm/s (average value over the distance of 30–35 cm). Fig. 4B compares the experimental LVP for that BSA solution with the average  $u_t$  ( $14.9 \pm 0.4$  cm/s), calculated from the data for the various low-molecular-weight surfactants in Fig. 2B for  $R = 0.73$  mm, and this comparison will be discussed further below.

## 3. Discussion

As mentioned earlier, the two identified features that distinguish the motion behavior of bubbles in protein from that in low-molecular-weight surfactant solutions have not been previously discussed in the literature, despite their potentially intriguing origins and implications to the general problem of the rising bubble dynamics. These phenomena warrant further investigation to understand better the mechanisms of the protein DAL formation at the rising bubble surface. Below, some hypotheses related to possible causes of this atypical bubble behavior are presented.

### 3.1. Potential bubble size increase in a liquid column

In experiments aimed at determining variations in the rising velocity of a single bubble and the kinetics of DAL formation, a bubble of air is typically generated using an orifice, such as a steel needle or glass capillary. The size of the orifice, under constant physicochemical conditions of the solution, determines the bubble's diameter. To calculate the diameter of the detaching bubble, a simple assumption balancing

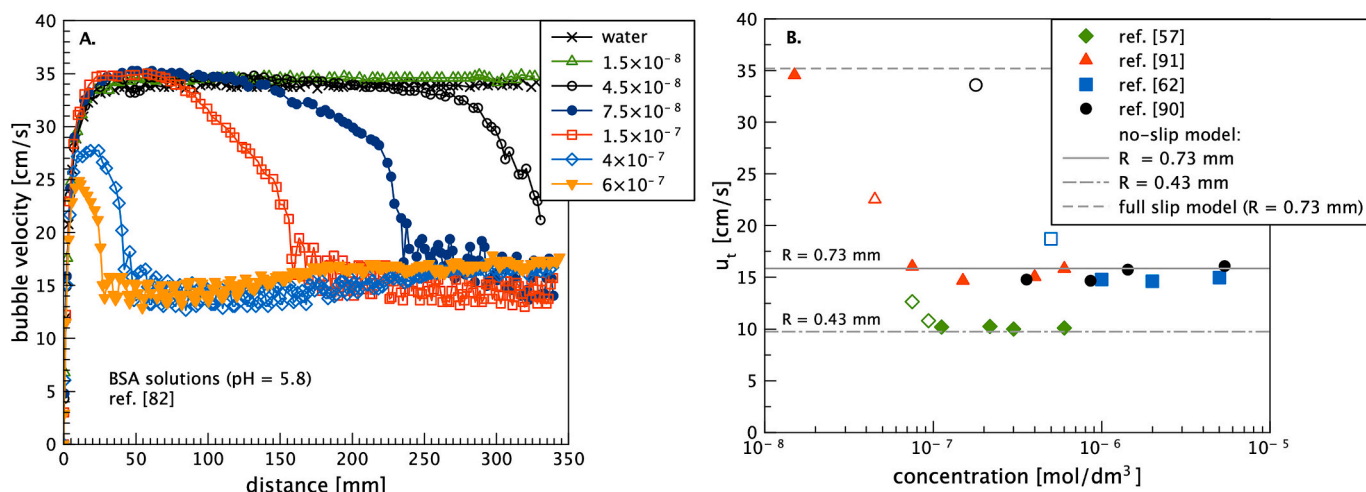


Fig. 3. Experimental results on (A) variations of local velocities of a bubble ( $R = 0.73$  mm) rising in BSA solutions of different concentrations and (B) bubble's terminal velocities  $u_t$  ( $R = 0.73$  and  $R = 0.43$  mm) in solutions of BSA (diamonds [57] and triangles [91]),  $\beta$ -lactoglobulin in 10 mM citric buffer at pH = 4 (squares [62], egg white protein (circles) [90]. In Fig. 3B error bars were not included to maintain clarity in the picture.

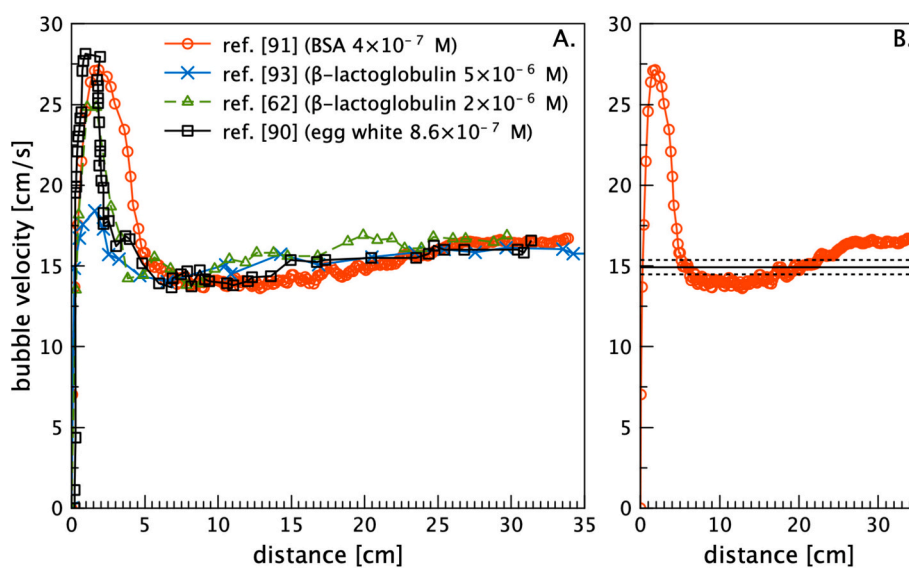


Fig. 4. Local velocity variations of a bubble (A) comparison of literature data for different proteins, (B) data for  $c_p = 4 \times 10^{-7}$  mol/dm<sup>3</sup> BSA solution [91], compared with average terminal velocity calculated basing on data from Fig. 2B (solid line – average terminal velocity, dashed lines – standard deviation).

buoyant ( $F_B$ ) and capillary ( $F_C$ ) forces can be considered, with  $F_C$  defined as:

$$F_C = \pi d_c \sigma \cos \theta \quad (7)$$

where  $\theta$  is a contact angle and  $d_c$  is an orifice diameter. Further,  $R$  can be calculated as:

$$R = \left( \frac{3d_c \sigma \cos \theta}{4\rho g} \right)^{1/3} \quad (8)$$

As reported earlier, Eq. (8) predicts the  $R$  value with high accuracy [78,94–96], assuming that the walls of the steel needle or glass capillary, used in typical experiments, are hydrophilic (air/orifice material contact angle equals to 0). That is typically the case in pure water or diluted aqueous solutions of surface-active species. While the orifice size remains constant throughout the experiment, the contact angle of the material from which it is constructed can vary depending on the solution's composition and surfactant concentration, particularly in the case of ionic surfactants. An increase in  $\theta$  for a given  $d_c$  theoretically causes a

linear decrease in  $R$ . However, in practice, for sufficiently concentrated solutions, this increase in  $\theta$  is often accompanied by an increase in the contact perimeter between the bubble and the capillary walls, which can lead to additional and sometimes significant increase in the size of the generated bubble. Such a situation was observed, for example, by Wiertel and Zawala [97,98], who studied the kinetics of single bubble attachment to a quartz surface in CTAB solutions. They controlled the initial adsorption coverage over the interface of the detaching bubble and observed that once a sufficiently high solution concentration was used, the size of the generated bubbles grew enormously. This finding was explained by the increase of the contact angle at the capillary wall surface due to electrostatically driven adsorption of positively charged CTAB molecules onto the negatively charged glass surface. This effect was particularly pronounced because a thick-walled capillary was used for bubble generation, with an inner diameter of only 0.075 mm but an outer diameter of 5.35 mm, which significantly increased the bubble/capillary attachment perimeter. A similar situation might be faced in the case of proteins. However, protein adsorption at hydrophilic solid surfaces often exhibits so-called overshooting adsorption kinetics, and the

adsorbed amounts for  $c_p$  in the  $\mu\text{M}$  range are relatively low [86,99]. Hence, the effect of solid surface hydrophobization by proteins is presumably comparable to the one exerted by CTAB, and therefore, it cannot be the reason for the observed subtle differences in the bubble motion behavior.

Moreover, typical experiments conducted to determine the LVPs of a bubble as a function of solution concentration are typically performed with the camera maintained in a stationary position and raised in discrete, short distances, dependent on the camera magnification. The camera captures images of successive bubbles released from the orifice. This method means that each LVP is created from segments determined by different bubbles. If present, the effect of increasing  $d_c$  values ( $\theta$  increase) could explain a smooth and continuous increase in bubble velocity. Initially, at the beginning of the experiment, the surface may be hydrophilic, but over time, it may gradually become hydrophobic, particularly at high  $c_p$ .

To test the validity of this hypothesis, an analysis of the rising bubble's geometrical parameters was performed using available (unpublished) data for both low-molecular-weight surfactants and BSA at  $c_p = 4 \times 10^{-7} \text{ mol/dm}^3$  (solution pH 5.8). The results are shown in Fig. 5<sup>1</sup>. The data points represent experimentally determined bubble geometrical parameters ( $d_h$ ,  $d_v$  and  $d_{eq}$ ), while the solid line is a linear regression fitted to the  $d_{eq}$  data to estimate the existence and magnitude of any potential bubble size increase. Values for water are included for comparison.

Using the parameters obtained by the fitted linear regression, the  $d_{eq}$  values were compared at two distances from the orifice ( $L$ ):  $L = 0 \text{ cm}$  (detaching bubble) and  $L = 30 \text{ cm}$  (the limit of the liquid column used). The magnitude of the bubble size increase was estimated, and the results are presented in Table 1., alongside the fitting parameters. As shown, the bubble size increase across the liquid column in various surface-active substances ranged between 1 % and 3 %. These values are reasonable, considering the accuracy of manual image analysis, slight deviations of the bubble trajectory from the focal plane, and consistency with the expected bubble expansion caused by the decrease in hydrodynamic pressure (which can be estimated using the ideal gas law as not larger than 1 %).

On the other hand, the increase in terminal velocity (from approximately 14 cm/s to 16.5 cm/s) observed at higher  $c_p$  (see Fig. 4) is around 15 %. Using the Schiller-Naumann model, it is seen that such a velocity increase would only be possible due to a corresponding bubble diameter change (15 %), which is not observed here. Therefore, our opinion is that the observed distinct velocity increase anomaly shown in Fig. 4 originates from a different cause and cannot be explained by changes in the bubble size, which can be safely neglected, as discussed above. Consequently, this intriguing effect should be entirely attributed to additional surface phenomena that influence the hydrodynamic boundary conditions at the liquid/gas interface. Such phenomena obviously originate from specificities of the protein DAL, which are still to be elucidated.

### 3.2. Adsorption dynamics and interfacial structure

It is well-known that the adsorption mechanism of proteins at interfaces is more complex than that of conventional surfactants. This complexity requires the development of complicated models for quantifying the protein adsorption process [35]. Generally, protein adsorption at a static liquid/fluid interface is considered to involve three main steps [36]: (i) diffusion of macromolecules from the bulk solution to the interface, (ii) adsorption and penetration into the adsorption layer, and

<sup>1</sup> The determination of bubble size and velocity through image analysis is usually subject to an error of approximately 1–2 pixels. In our experiments (unpublished data used in the paper), this uncertainty ranged from 10 to 70  $\mu\text{m}$ , depending on the camera magnification.

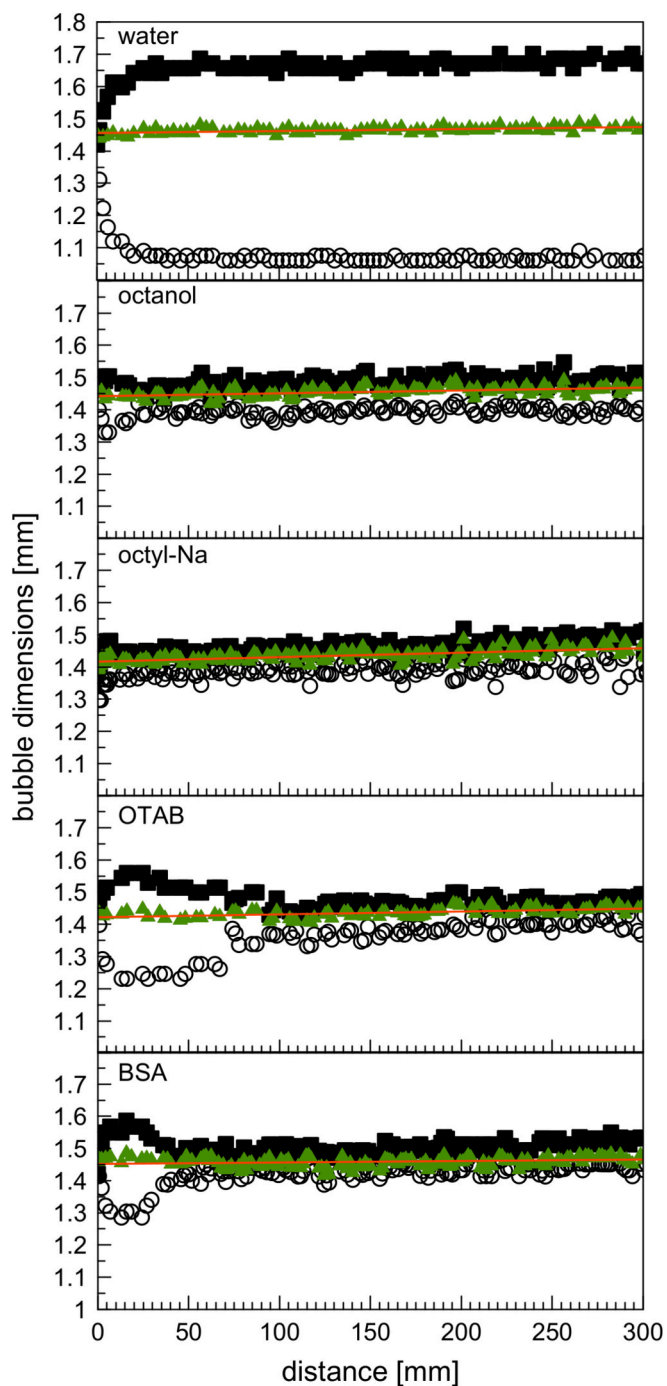


Fig. 5. Variations of the rising bubble geometrical parameters ( $d_h$  – full squares,  $d_v$  – open circles,  $d_{eq}$  – full green triangles) as a function of distance from the orifice in solutions of several low-molecular-weight surfactants and BSA (unpublished data). The solution concentrations are given in Table 1.

(iii) rearrangement of the adsorbed proteins at the gas/liquid interface; the latter two steps may induce structural deformations of protein globules due to interactions with the surface [33]. Moreover, unlike low-molecular-weight surfactants, whose adsorption at the liquid/air interface is reversible, protein desorption is governed by a barrier mechanism and slow desorption kinetics, suggesting that protein adsorption is largely irreversible [100–102].

The tendency of a protein to adsorb irreversibly at a static liquid/gas interface may also be valid in the case of the surface of a rising bubble. This hypothesis can explain the absence of a “transient zone” (partial

**Table 1**

Linear regression fitting parameters used to estimate the magnitude of bubble size increase along a liquid column of length 30 cm for different surface-active species, based on the data presented in Fig. 5.

	$c$ [mol/ dm <sup>3</sup> ]	$a \times$ $10^{-5}$	$b$ [mm] ( $d_{eq}$ for $L =$ 0)	$d_{eq}$ , [mm] (for $L = 30$ cm)	% of increase
water	–	6.27	1.46	1.48	1.3
octanol	$3 \times 10^{-5}$	8.85	1.44	1.47	1.8
octyl- Na	$1 \times 10^{-2}$	13.9	1.42	1.46	2.9
OTAB	$5 \times 10^{-2}$	8.98	1.42	1.45	1.9
BSA	$4 \times 10^{-7}$	4.61	1.45	1.46	1.0

surface immobilization) in the  $u_t(c_p)$  dependencies (as shown in Fig. 3 and discussed therein). Due to the inhibited desorption of protein molecules, their continuous accumulation on the bubble surface leads to a gradual increase in the adsorption coverage and the formation of an extended stagnant cap over the bubble surface ( $\psi \rightarrow 180^\circ$ ). This effect is expected to weaken eventual surface tension gradients and thus to decrease the drag coefficient, resulting in partial and slight remobilization of the bubble surface. This hypothesis is strongly supported by results on the dependence of the travel distance  $L_{DAL}$  (at which  $u_t$  is established under steady-state conditions and a complete DAL structure is formed) as a function of  $c_p$ . Such results, based on selected literature data, are shown in Fig. 6. The observed differences in the  $L_{DAL}$  vs.  $c_p$  data clearly confirm that rate of accumulation of protein molecules at a bubble surface is concentration dependent and distance (time) needed for  $u_t$  establishment decreases when solution concentration increases.

Similar conclusions were drawn in a recent theoretical study by Wang et al. [70], who examined the effects of adsorption, desorption, and diffusion characteristics of surfactants on the hydrodynamic properties of a bubble in a surfactant solution at moderate Reynolds numbers. Based on CFD simulations, it was demonstrated that an increase in the Langmuir number ( $La$ ), defined as  $La = k_a \cdot c / k_d$ , where  $k_a$  and  $k_d$  are adsorption and desorption rate constants, respectively, i.e., either an increase of  $k_a$  or a decrease of  $k_d$  leads to an increase of the stagnant cap angle  $\psi$  and thereby of the interfacial concentration. It was reported that when  $La$  increased from 0.02 to 0.09,  $\psi$  increased from  $60^\circ$  to  $180^\circ$  (i.e. the entire bubble surface is covered by an adsorption layer in the geometry used in the study). Further increase in  $La$  from 0.09 to

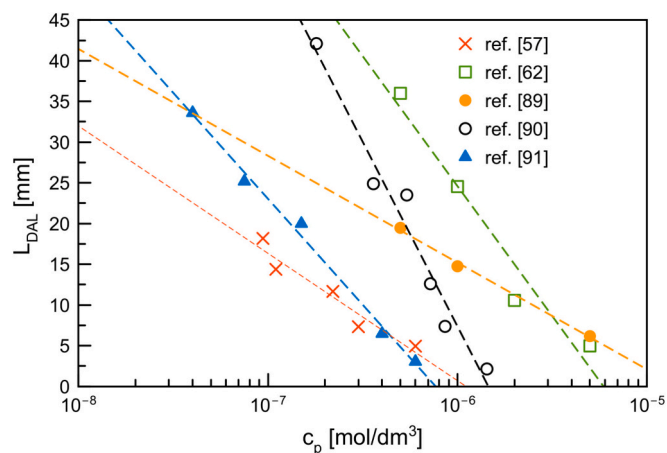


**Fig. 6.** Distance ( $L_{DAL}$ ), at which terminal velocity ( $u_t$ ) is established (full DAL architecture is formed) as a function of protein solution concentration ( $c_p$ ) for: BSA (crosses [57] and full triangles [91])  $\beta$ -lactoglobulin in 10 mM buffer pH 4 [62] (open squares), egg white protein in water [90] (open circles) and  $\beta$ -casein in water [89] (full circles). Error bars were not included to maintain clarity in the picture.

0.6 did not change  $\psi$ , but were associated with a pronounced increase in the interfacial concentration. With an increase in  $La$  from 0.09 to 0.28, the interfacial concentration continuously increased while the interfacial tangential velocity remained almost unchanged. However, when the  $La$  number increased from 0.28 to 0.6, the interfacial tangential velocity also increased, indicating an increase in the bubble's rising velocity.

Concerning the molecular structure of a protein DAL and its implications for bubble motion dynamics, relations to the current state-of-the-art of our understanding of protein architectures at static liquid/gas interfaces [33] are still to be identified and investigated. It is well accepted that a protein globule may undergo structural deformation upon adsorption at a static liquid/gas interface. The intensity of this process depends on intrinsic molecular properties such as flexibility/rigidity of the tertiary protein structure and the protein net charge as modulated by changes in the environmental conditions [33]. Furthermore, the time evolution of such structural molecular transformations is expected to vary for different proteins and environmental conditions, however, the relevant rate constants are yet unknown. The main problem with translating these interfacial processes from the condition of a static interface to the surface of a rising bubble is the much shorter time scale and the intense hydrodynamics in rising bubble experiments. In this connection, we performed a dedicated experiment, which is explained in the following paragraph.

Fig. 7 presents a comparison of the LVPs for air bubbles in a BSA solution at relatively high  $c_p = 6 \times 10^{-7}$  mol/dm<sup>3</sup>, measured using the setup described in detail in [94,97,98]. This setup allows for precise control of the initial adsorption coverage on the surface of the releasing bubble. Briefly, the setup enables a bubble to be held static for a controlled time in a trap (a glass dome attached to a stepper motor). During this period, the bubble surface is continuously exposed to surface-active molecules diffusing from the solution. After the selected adsorption time, the bubble is released to rise in the liquid column. Fig. 7 includes data from [91], which are compared with a new set of results (unpublished data) obtained with and without adsorption time control in a significantly longer liquid column (65 cm). Notably, an excellent correlation was found between the literature data and the newly obtained data for the case of no-trap experiments, which reveal a clear increase of  $u$  following the establishment of  $u_t$ . It can be noted that once a terminal velocity of approximately 16–16.5 cm/s is reached at  $L \approx 20$  cm, it remains constant until the end of the experiment. When a bubble trap is used, the bubble's velocity profile differs significantly. The acceleration-deceleration peak at the LVP disappears, and terminal velocity is reached almost instantly after the moment of the bubble's

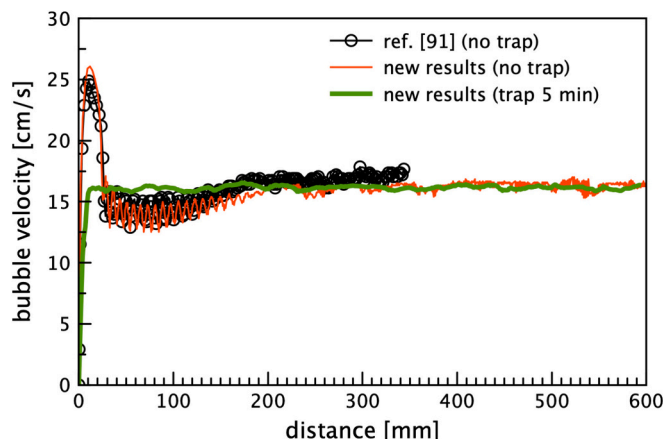


**Fig. 7.** Comparison of LVPs for air bubbles in a BSA solution at  $c_p = 6 \times 10^{-7}$  mol/dm<sup>3</sup> in pure water measured in the bubble trap setup with and without adsorption time control (for details see in the main text). Literature data reported in [91] are shown alongside the recently obtained new results in a 65 cm long liquid column (unpublished data).

release, matching the velocity observed after the increase in the no-trap scenario. In both cases, however, terminal velocity is higher than that expected for a bubble with full no-slip surface. These findings support the results of simulations presented in [70] characteristics under dynamic conditions in light of interfacial mobility.

In summary, based on the state-of-the-art knowledge of the motion dynamics of air bubbles in aqueous solutions of low-molecular-weight surfactants, new features were identified in the general LVP of air bubbles in protein solutions (schematized in Fig. 8):

- Lack of intermediate terminal velocities, i.e., a protein DAL is not capable of creating partial slip conditions at the rising bubble surface;
- The terminal velocity at fully developed protein DAL cannot be explained by existing theories – new theoretical approaches are urgently needed;
- A local minimum in the LVP is observed at relatively high  $c_p$ , which should be related to a transient stage in the bubble motion dynamics induced by specificities of the protein DAL dynamics and structure.

These new findings necessitate phenomenological development of the physicochemical problem of a rising bubble in solution accounting for additional interfacial processes and phenomena induced by macromolecules, which are not observed for low-molecular-weight surfactants. Despite the evident effect of re-mobilization of the bubble surface in protein solutions at relatively high  $c_p$  – likely due to weakened surface tension gradients on the rising bubble surface – there are still open questions that need to be addressed in future investigations involving macromolecular surfactants (such as proteins and polymers). Some of these pending questions, which await experimental and/or theoretical verification, are listed below:

- Is the increase of  $u_t$  above the theoretical predictions (valid for the case of low-molecular-weight surfactants) solely caused by weakened surface tension gradients and a distinct DAL structure (compared to low-molecular-weight surfactants)? Is this the only mechanism involved?
- If this velocity increase is due to weakened surface tension gradients that lead to a reduced drag coefficient, why is it limited to  $\sim 2$  cm/s (to ca. 16–16.5 cm/s, even for longer distances, as shown in Fig. 7)?
- Does a viscoelastic network form over the bubble surface when the compression zone is gradually built up? Could this be the reason for the decrease in the drag coefficient and the increase in interfacial tangential velocity?
- In general, how do influencing factors such as size, charge, and the molecular structure of a protein globule impact the dynamics of these new processes and phenomena?

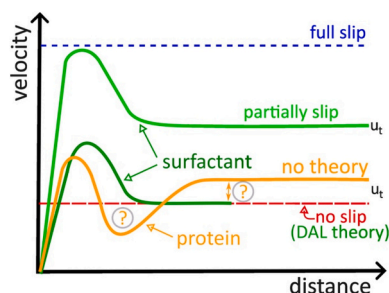


**Fig. 8.** Schematic representation of the general shapes of LVPs for bubbles in solutions of low-molecular-weight surfactants or proteins. The boundary conditions of full-slip and no-slip, defined by models (verified by experimental data for low-molecular-weight surfactants), are depicted by dashed lines; solid lines are virtual LVPs;  $u_t$  is bubble terminal velocity. The question marks emphasize specific features in the protein LVP.

#### 4. Additional proof for different DAL structure in protein solution and its consequences for single foam films stability

In the case of low-molecular-weight surfactants, the presence of DAL was confirmed in experiments that evaluated the stability of an individual foam film [48,49,103–106] or wetting film [51,97,107,108] formed at the collision of a bubble with a liquid/gas or a liquid/solid interface. The model system of a single liquid film has been employed as a sensitive tool to probe the properties of liquid/gas interfaces, providing experimental evidence for the existence of the DAL at the rising bubble interface and its impact on the process of film drainage. In these experiments, the travel distance ( $L$ ) between the bubble formation point (orifice) and the liquid/air or liquid/solid interface was varied to monitor different stages of the DAL development (see Fig. 9). For foam films, which form between a bubble and a liquid/gas interface, two liquid column lengths were tested: a “short” column ( $L$  of a few centimeters) and a “long” column ( $L$  ranging from 15 to 40 cm). The findings showed that the lifetime of the foam film created by the colliding bubble was notably shorter in the “long” column, even though it was anticipated that a longer travel distance through the liquid column would lead to a higher equilibrium adsorption coverage at the bubble’s surface. This finding suggests that, despite the increased surface coverage, the liquid film drained faster in the “long” column, which fact was used to argue for greater interface mobility and the existence of a region with lower surfactant coverage at the bubble’s apex. This scenario is illustrated in Fig. 10 by literature data on the lifetime of foam films as a function of the solution concentration for several low-molecular-weight surfactants. It is essential to note the rich statistics gained in these experiments – each data point in Fig. 10 represents an average value calculated from 100 to 250 individual bubbles. This achievement was made possible by employing a setup with automatic lifetime registration via a video camera and a precise protocol for releasing subsequent bubbles from the orifice, with the release interval adjusted to match the lifetime magnitude.

Direct quantitative evidence demonstrating this effect was presented in reference [106] basing on drainage kinetics data obtained using the Dynamic Fluid-Film Interferometry (DFI) technique in a setup with modified geometry (with freely rising bubbles). Selected data on the evolution of the liquid film thickness for both “short” (1 cm) and “long” (40 cm) columns from ref. [106] are presented in Fig. 11. The horizontal dashed line (set at 100 nm) is included for clarity and highlights the

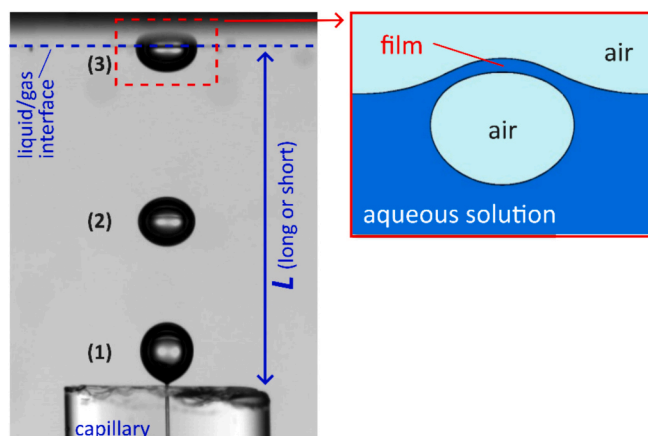


**Fig. 9.** Illustration of an experiment designed to assess the stability of a foam film by measuring the lifetime of a single bubble at the free surface of an aqueous solution. The experiment involved the following steps: a bubble was grown and detached from a capillary or needle (1), followed by its free rise (2) through a liquid column of varying lengths (“long” or “short”). Upon reaching the free surface of the solution, the bubble collided with it and formed a liquid film (3). The bubble’s lifetime, directly linked to the drainage dynamics of the film, was measured using an automated acquisition system [48,49,103–106].

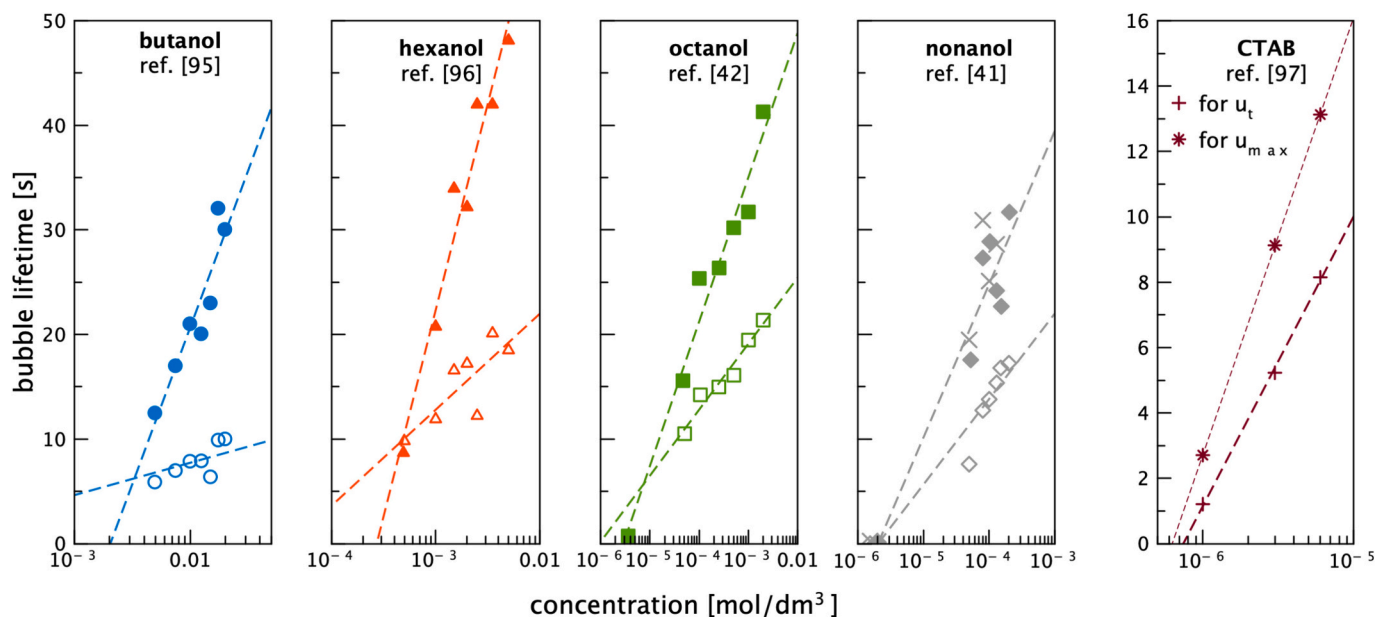


**Fig. 10.** Lifetimes of a single bubble at free solution surface (foam film) in different alkanols solutions: hollow symbols –  $L = 39.5$  cm, solid symbols –  $L = 4$  cm,  $\times$  –  $L = 1$  cm. In the ref. [105] the solution surface position was adjusted to capture either maximum ( $u_{max}$ ) or terminal ( $u_t$ ) velocity, depending on the solution concentration (error bars were not included to maintain clarity in the picture). Lines are analytical function  $[y = a \bullet \log(x) + b]$  fits to the experimental data.

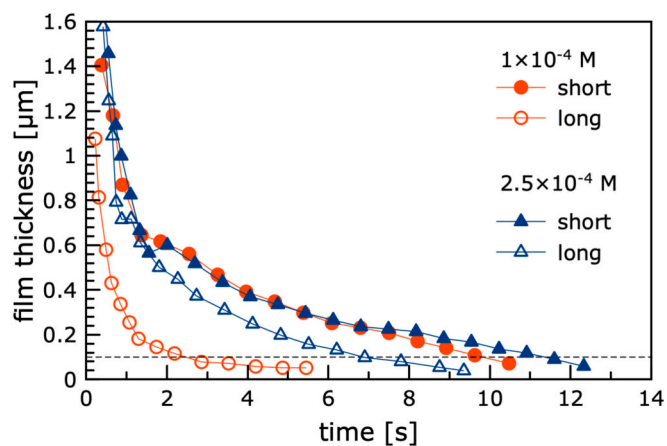


**Fig. 11.** Time evolution of the foam film thickness for short and long columns (solution of n-octanol of two chosen concentrations) for  $R = 1$  mm. Redrawn basing on data taken from ref. [106]. Horizontal dashed line denotes thickness equal to 100 nm (thickness accuracy measurement  $\pm 20$  nm).

faster drainage of the liquid film in the “long” column compared to the “short” one. In addition, it was shown in [106] that for “short” column, the reestablishment of uniform adsorption coverage – and the corresponding decrease in interfacial mobility – is related to the reorganization of surfactant molecules induced by higher bubble impact velocities and an increased tendency for bouncing.

Similar data to those shown in Figs. 10 and 11, obtained under comparable conditions, have never been reported for protein solutions. To enable a comparison of foam film stability between different groups of surface-active species, as discussed in this paper, we present unpublished data from our laboratories. The experiments with BSA solutions in pure water and at varying  $c_p$  replicate those described in ref. [30] (all details about the equipment used, experimental protocol and the data analysis methods can be found in ref. [106] and in the supplementary information provided in Appendix A of the referenced paper). A BoD (Bubble-on-Demand) generator [94] was used to control the time interval of bubble release from a steel needle with a diameter of 0.21 mm.

The equivalent bubble radius was  $1.04 \pm 0.04$  mm.

Fig. 12 presents sequences of photographic snapshots (DFI method) taken during the drainage of films (BSA concentration of  $5 \times 10^{-6}$  mol/dm<sup>3</sup>) in experiments with the “short” and the “long” columns. The images correspond to comparable drainage times, and the color scale bar on the right-hand side illustrates the film thickness distribution in microns. The time of bubble/solution surface collision was set to  $t = 0$  s. As observed, the foam films formed in both cases ( $L = 1$  cm and  $L = 40$  cm) are highly inhomogeneous in thickness. Similar characteristics of foam films in protein solutions have been reported previously for films formed under quasi-static conditions [109–112]. A relatively large, thick area initially located in the film’s center shifts toward its rim over time, exposing thinner regions. Eventually, at the point of rupture (as seen in the last images of each row), black areas become visible in the film, indicating that the thickness in these spots has dropped below approximately 50 nm. Moreover, it is evident that film drainage occurs faster in the “long” column (as seen in the images around 14–15 s), which is the opposite of what is typically observed in solutions of low-molecular-weight surfactants (see Figs. 10 and 11, and results in [106]).

Fig. 13 presents the average film lifetimes for BSA solutions at different concentrations. These values were obtained using the reproduced method described in references [49, 105]. For each concentration, the average lifetime was calculated based on 100 individual measurements. The bubble size and the two positions of the solution surface relative to the orifice were identical to those used in the DFI experiments. The effect is evident: above a certain threshold concentration ( $c_p > 10^{-6}$  mol/dm<sup>3</sup>), the film lifetime, and thus its stability, is significantly higher for the “long” column. That supports the hypothesis that the structure of protein DAL differs from of what is typically expected for low-molecular-weight surfactants. In particular, likely, the depletion zone at the bubble apex does not exist in this case, and instead, the apex is covered by protein molecules. The degree of coverage, which determines the surface mobility, depends on the time the bubble travels in the liquid column.

## 5. Conclusions

This review has highlighted significant differences in the motion behavior of rising bubbles in solutions of low-molecular-weight

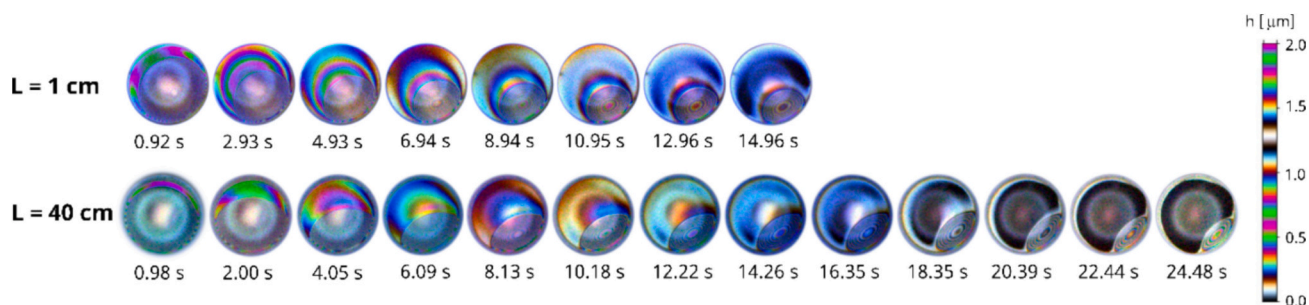


Fig. 12. Images of foam films formed by a bubble ( $R = 1$  mm) colliding with the free surface of a BSA solution ( $c_p = 5 \times 10^{-6}$  mol/dm<sup>3</sup>), captured using the DFI method (unpublished data).

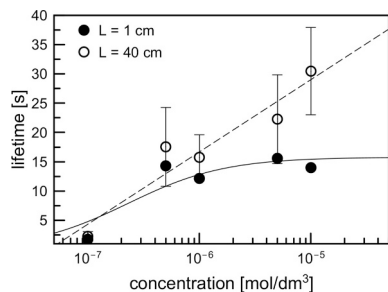


Fig. 13. Average lifetimes of single floating bubbles ( $R = 1$  mm) at the free solution surface (foam film) in BSA solutions of varying concentrations (“short” column  $L = 1$  cm – solid symbols, “long” column  $L = 40$  cm – hollow symbols; unpublished data). Lines are guides to the eye.

surfactants or proteins, providing deeper insights into the formation of the Dynamic Adsorption Layer (DAL) at liquid/gas interfaces. The differences in the DAL architecture between surfactants and proteins are emphasized, based on available literature and supported by recently obtained (unpublished) experimental data from our laboratories. In surfactant solutions, DAL formation occurs more predictably, with partial immobilization of the interface, allowing for a gradual transition in bubble mobility. In contrast, protein solutions can induce complete immobilization of the bubble surface without any transient zones, likely due to irreversible adsorption. Moreover, bubble behavior in protein solutions – particularly the re-mobilization of the bubble surface at relatively high protein concentrations – suggests complex interfacial dynamics. This re-mobilization seems to arise from weakened surface tension gradients and results in unique velocity profiles. Furthermore, there are indications that the protein molecular properties may play a significant role. However, this hypothesis needs to be verified by more detailed investigations. We believe that combining experimental techniques with Computational Fluid Dynamics (CFD) offers promising opportunities for deeper exploration, particularly in understanding the complex interactions between surface-active molecule adsorption, bubble dynamics, and DAL formation. Furthermore, the study encourages further investigation of the adsorption properties of macromolecular surfactants with diverse molecular structures to enhance comprehension of the structure-property relationships associated with the rising bubble phenomenon.

#### CRediT authorship contribution statement

**L. Witkowski:** Writing – review & editing, Writing – original draft, Validation, Software, Formal analysis, Data curation, Conceptualization. **A. Wiertel-Pochopien:** Writing – review & editing, Writing – original draft, Visualization, Methodology, Formal analysis. **D. Kosior:** Writing – review & editing, Writing – original draft, Supervision, Methodology, Data curation, Conceptualization. **G. Gochev:** Writing – review &

editing, Writing – original draft, Formal analysis, Conceptualization. **P. Warszynski:** Writing – review & editing, Conceptualization. **G.G. Fuller:** Writing – review & editing, Supervision, Conceptualization. **J. Zawala:** Writing – original draft, Supervision, Software, Methodology, Funding acquisition, Formal analysis, Data curation, Conceptualization.

#### Declaration of competing interest

Jan Zawala reports financial support was provided by National Science Centre Poland.

#### Acknowledgements

Partial financial support from the Polish National Science Centre (NCN grant no. 2021/43/B/ST8/00053) and statutory research fund of ICSC PAS is acknowledged with gratitude. J.Z. expresses gratitude to Kazimierz Malysa and Reinhard Miller for the opportunity to witness their numerous insightful discussions on LVPs in protein solutions, which served as an inspiration for this work.

#### Data availability

Data will be made available on request.

#### References

- Cho YS, Laskowski JS. Effect of flotation frothers on bubble size and foam stability. *Int J Miner Process* 2002;64:69–80. [https://doi.org/10.1016/S0301-7516\(01\)00064-3](https://doi.org/10.1016/S0301-7516(01)00064-3).
- Karakashev SI, Stöckelhuber KW, Tsekov R, Phan CM, Heinrich G. Tribology of thin wetting films between bubble and moving solid surface. *Adv Colloid Interf Sci* 2014;210:39–46. <https://doi.org/10.1016/j.cis.2013.10.019>.
- Murray BS. Recent developments in food foams. *Curr Opin Colloid Interface Sci* 2020;50:101394. <https://doi.org/10.1016/j.cocis.2020.101394>.
- Sheng Y, Xue M, Ma L, Zhao Y, Wang Q, Liu X. Environmentally friendly firefighting foams used to fight flammable liquid fire. *Fire Technol* 2021;57:2079–96. <https://doi.org/10.1007/S10694-021-01115-Z/FIGURES/10>.
- Schad T, Preisig N, Drenckhan W, Stubenrauch C. Foam-based cleaning of surfaces contaminated with mixtures of oil and soot. *J Surfactant Deterg* 2022;25:377–85. <https://doi.org/10.1002/JSDE.12580>.
- Arzhavitina A, Steckel H. Foams for pharmaceutical and cosmetic application. *Int J Pharm* 2010;394:1–17. <https://doi.org/10.1016/J.IJPHARM.2010.04.028>.
- Hoc D, Haznar-Garbacz D. Foams as unique drug delivery systems. *Eur J Pharm Biopharm* 2021;167:73–82. <https://doi.org/10.1016/J.EJPB.2021.07.012>.
- Badmus SO, Amusa HK, Oyehan TA, Saleh TA. Environmental risks and toxicity of surfactants: overview of analysis, assessment, and remediation techniques. *Environ Sci Pollut Res* 2021;28:44 2021;28:62085–104. doi:<https://doi.org/10.1007/S11356-021-16483-W>.
- Farias CBB, Almeida FCG, Silva IA, Souza TC, Meira HM, Soares da Silva R, et al. Production of green surfactants: market prospects. *Electron J Biotechnol* 2021;51:28–39. <https://doi.org/10.1016/J.EJBT.2021.02.002>.
- Nagtode VS, Cardoza C, Yasin HKA, Mali SN, Tambe SM, Roy P, et al. Green surfactants (biosurfactants): a petroleum-free substitute for sustainability—comparison, applications, market, and future prospects. *ACS Omega* 2023;8:11674–99. [https://doi.org/10.1021/ACSOMEGA.3C00591/ASSET/IMAGES/LARGE/AO3C00591\\_0011.JPEG](https://doi.org/10.1021/ACSOMEGA.3C00591/ASSET/IMAGES/LARGE/AO3C00591_0011.JPEG).
- Sriniv SSSS, Riniv R, Rinivasan R, Asan Asan Asan DDDA, Damodaran D, Amodaran A. Protein stabilization of emulsions and foams. *J Food Sci* 2005;70:R54–66. <https://doi.org/10.1111/J.1365-2621.2005.TB07150.X>.

- [12] Amagliani L, Silva JVC, Saffon M, Dombrowski J. On the foaming properties of plant proteins: current status and future opportunities. *Trends Food Sci Technol* 2021;118:261–72. <https://doi.org/10.1016/j.tifs.2021.10.001>.
- [13] Wierenga PA, Gruppen H. New views on foams from protein solutions. *Curr Opin Colloid Interface Sci* 2010;15:365–73. <https://doi.org/10.1016/j.cocis.2010.05.017>.
- [14] Gehle RD, Schügerl K. Protein recovery by continuous flotation. *Appl Microbiol Biotechnol* 1984;20:133–8. <https://doi.org/10.1007/BF00252591/METRICS>.
- [15] Lockwood CE, Bummer PM, Jay M. Purification of proteins using foam fractionation. *Pharm Res* 1997;14:1511–5. <https://doi.org/10.1023/A:1012109830424/METRICS>.
- [16] Brown AK, Kaul A, Varley J. Continuous foaming for protein recovery: part I. Recovery of casein. *Biotechnol Bioeng* 1999;62:278–90. [https://doi.org/10.1002/\(SICI\)1097-0290\(19990205\)62:3](https://doi.org/10.1002/(SICI)1097-0290(19990205)62:3).
- [17] Brown AK, Kaul A, Varley J. Continuous Foaming for Protein Recovery: Part II. Selective Recovery of Proteins from Binary Mixtures. 1999. [https://doi.org/10.1002/\(SICI\)1097-0290\(19990205\)62:3](https://doi.org/10.1002/(SICI)1097-0290(19990205)62:3).
- [18] Sebba F. Biliquid foams—a preliminary report. *J Colloid Interface Sci* 1972;40:468–74. [https://doi.org/10.1016/0021-9797\(72\)90356-6](https://doi.org/10.1016/0021-9797(72)90356-6).
- [19] Jauregi P, Varley J. Colloidal gas Aphrons: a novel approach to protein recovery. *Biotechnol Bioeng* 1998;59:471–81. [https://doi.org/10.1002/\(SICI\)1097-0290\(19980820\)59:4](https://doi.org/10.1002/(SICI)1097-0290(19980820)59:4).
- [20] Noble M, Brown A, Jauregi P, Kaul A, Varley J. Protein recovery using gas–liquid dispersions. *J Chromatogr B Biomed Sci Appl* 1998;711:31–43. [https://doi.org/10.1016/S0378-4347\(98\)0030-9](https://doi.org/10.1016/S0378-4347(98)0030-9).
- [21] Jarudilokkul S, Rungphetcharat K, Boonamnuyvitaya V. Protein separation by colloidal gas aphrons using nonionic surfactant. *Sep Purif Technol* 2004;35:23–9. [https://doi.org/10.1016/S1383-5866\(03\)00111-4](https://doi.org/10.1016/S1383-5866(03)00111-4).
- [22] Pal P, Hasan SW, Abu Haija M, Sillanpää M, Banat F. Colloidal gas aphrons for biotechnology applications: a mini review. *Crit Rev Biotechnol* 2023;43:971–81. <https://doi.org/10.1080/07388551.2022.2092716>.
- [23] Brunner CA, Stephan DG. Foam fractionation. *Ind Eng Chem* 1965;57:40–8. <https://doi.org/10.1021/IE50665A008/ASSET/IE50665A008.FP.PNG.V03>.
- [24] Lemlich R. Adsorptive bubble separation methods: foam fractionation and allied techniques. *Ind Eng Chem* 1968;60:16–29. <https://doi.org/10.1021/IE50706A005/ASSET/IE50706A005.FP.PNG.V03>.
- [25] Buckley T, Xu X, Rudolph V, Firouzi M, Shukla P. Review of foam fractionation as a water treatment technology. *Sep Sci Technol* 2022;57:929–58. <https://doi.org/10.1080/01496395.2021.1946698>.
- [26] We ACE, Zamyadi A, Stickland AD, Clarke BO, Freguia S. A review of foam fractionation for the removal of per- and polyfluoroalkyl substances (PFAS) from aqueous matrices. *J Hazard Mater* 2024;465:133182. <https://doi.org/10.1016/j.jhazmat.2023.133182>.
- [27] Wong CH, Hossain MM, Davies CE. Performance of a continuous foam separation column as a function of process variables. *Bioprocess Biosyst Eng* 2001;24:73–81. <https://doi.org/10.1007/S004490100225/METRICS>.
- [28] Oraby A, Weickardt I, Zibek S. Foam fractionation methods in aerobic fermentation processes. *Biotechnol Bioeng* 2022;119:1697–711. <https://doi.org/10.1002/BIT.28102>.
- [29] Linke D, Berger RG. Foaming of proteins: new prospects for enzyme purification processes. *J Biotechnol* 2011;152:125–31. <https://doi.org/10.1016/j.jbiotec.2010.07.022>.
- [30] Zhang Y, Di R, Zhang H, Zhang W, Wu Z, Liu W, et al. Effective recovery of casein from its aqueous solution by ultrasonic treatment assisted foam fractionation: inhibiting molecular aggregation. *J Food Eng* 2020;284:110042. <https://doi.org/10.1016/j.jfoodeng.2020.110042>.
- [31] Keshavarzi B, Krause T, Sikandar S, Schwarzenberger K, Eckert K, Ansoerge-Schumacher MB, et al. Protein enrichment by foam fractionation: experiment and modeling. *Chem Eng Sci* 2022;256:117715. <https://doi.org/10.1016/j.ces.2022.117715>.
- [32] Chandran Suja V, Rodríguez-Hakim M, Tajuelo J, Fuller GG. Single bubble and drop techniques for characterizing foams and emulsions. *Adv Colloid Interf Sci* 2020;286. <https://doi.org/10.1016/j.cis.2020.102295>.
- [33] Gochev GG, Campbell RA, Schneck E, Zawala J, Warszynski P. Exploring proteins at soft interfaces and in thin liquid films – from classical methods to advanced applications of reflectometry. *Adv Colloid Interf Sci* 2024;329:103187. <https://doi.org/10.1016/j.cis.2024.103187>.
- [34] Razumovsky L, Damodaran S. Surface activity–compressibility relationship of proteins at the air–water interface. *Langmuir* 1999;15:1392–9. <https://doi.org/10.1021/LA980873V>.
- [35] Liggieri L, Mileva E, Miller R. The surface layer as the basis for foam formation and stability. *Foam Films Foams* 2018;3–55. <https://doi.org/10.1201/9781351117746-1>.
- [36] Zhou B, Tobin JT, Drusch S, Hogan SA. Interfacial properties of milk proteins: a review. *Adv Colloid Interf Sci* 2021;295. <https://doi.org/10.1016/j.cis.2020.102347>.
- [37] Reinhard Miller, Liggieri L. *Interfacial Rheology*. 2019.
- [38] Hénon S, Meunier J. Microscope at the Brewster angle: direct observation of first-order phase transitions in monolayers. *Rev Sci Instrum* 1991;62:936–9. <https://doi.org/10.1063/1.1142032>.
- [39] Engelhardt K, Peukert W, Braunschweig B. Vibrational sum-frequency generation at protein modified air–water interfaces: effects of molecular structure and surface charging. *Curr Opin Colloid Interface Sci* 2014;19:207–15. <https://doi.org/10.1016/j.cocis.2014.03.008>.
- [40] Hosseinpour S, Roeters SJ, Bonn M, Peukert W, Woutersen S, Weidner T. Structure and dynamics of interfacial peptides and proteins from vibrational sum-frequency generation spectroscopy. *Chem Rev* 2020;120:3420–65. [https://doi.org/10.1021/ACS.CHEMREV.9B00410/ASSET/IMAGES/MEDIUM/CR9B00410\\_0039.GIF](https://doi.org/10.1021/ACS.CHEMREV.9B00410/ASSET/IMAGES/MEDIUM/CR9B00410_0039.GIF).
- [41] Ekserova DR, Georgi Gochev, Platanikov D, Liggieri L, Reinhard Miller. *Foam Films and Foams : Fundamentals and Applications*. CRC Press; 2021.
- [42] Chatzigiannakis E, Jaensson N, Vermant J. Thin liquid films: where hydrodynamics, capillarity, surface stresses and intermolecular forces meet. *Curr Opin Colloid Interface Sci* 2021;53:101441. <https://doi.org/10.1016/j.cocis.2021.101441>.
- [43] Chang CH, Franses EI. Adsorption dynamics of surfactants at the air/water interface: a critical review of mathematical models, data, and mechanisms. *Colloids Surf A Physicochem Eng Asp* 1995;100:1–45. [https://doi.org/10.1016/0927-7757\(94\)03061-4](https://doi.org/10.1016/0927-7757(94)03061-4).
- [44] Peng M, Duignan TT, Nguyen CV, Nguyen AV. From surface tension to molecular distribution: modeling surfactant adsorption at the air–water interface. *Langmuir* 2021;37:2237–55. [https://doi.org/10.1021/ACS.LANGMUIR.0C03162/ASSET/IMAGES/LARGE/LA0C03162\\_0004.JPEG](https://doi.org/10.1021/ACS.LANGMUIR.0C03162/ASSET/IMAGES/LARGE/LA0C03162_0004.JPEG).
- [45] Dalkas G, Euston SR. Molecular simulation of protein adsorption and conformation at gas–liquid, liquid–liquid and solid–liquid interfaces. *Curr Opin Colloid Interface Sci* 2019;41:1–10. <https://doi.org/10.1016/j.cocis.2018.11.007>.
- [46] Aaroen O, Riccardi E, Erp TS van, Sletmoen M. Thin film breakage in oil–in–water emulsions, a multidisciplinary study. *Colloids Surf A Physicochem Eng Asp* 2022; 632:127808. doi:<https://doi.org/10.1016/j.colsurfa.2021.127808>.
- [47] Malysa K, Lunkenheimer K. Foams under dynamic conditions. *Curr Opin Colloid Interface Sci* 2008;13:150–62. <https://doi.org/10.1016/j.cocis.2007.11.008>.
- [48] Warszyński P, Jachimska B, Malysa K. Experimental evidence of the existence of non-equilibrium coverages over the surface of the floating bubble. *Colloids Surf A Physicochem Eng Asp* 1996;108:321–5. [https://doi.org/10.1016/0927-7757\(95\)03400-5](https://doi.org/10.1016/0927-7757(95)03400-5).
- [49] Jachimska B, Warszyński P, Malysa K. Influence of Adsorption Kinetics and Bubble Motion on Stability of the Foam Films Formed at n-Octanol, n-Hexanol and n-Butanol Solution Surface vol. 192. 2001.
- [50] Malysa K, Krasowska M, Krzan M. Influence of surface active substances on bubble motion and collision with various interfaces. *Adv Colloid Interf Sci* 2005; 114–115:205–25. <https://doi.org/10.1016/j.cis.2004.08.004>.
- [51] Zawala J, Kosior D, Malysa K. Formation and influence of the dynamic adsorption layer on kinetics of the rising bubble collisions with solution/gas and solution/solid interfaces. *Adv Colloid Interf Sci* 2015;222:765–78. <https://doi.org/10.1016/j.cis.2014.07.013>.
- [52] Levich VG. *Physicochemical Hydrodynamics*. Prentice-Hall; 1962.
- [53] Dukhin SS, Miller R, Loglio G. Physico-chemical hydrodynamics of rising bubble. In: *Studies in Interface Science*. vol. 6. Elsevier; 1998. p. 367–432. [https://doi.org/10.1016/S1383-7303\(98\)80025-2](https://doi.org/10.1016/S1383-7303(98)80025-2).
- [54] Krzan M, Zawala J, Malysa K. Development of steady state adsorption distribution over interface of a bubble rising in solutions of n-alkanols (C5, C8) and n-alkyltrimethylammonium bromides (C8, C12, C16). *Colloids Surf A Physicochem Eng Asp* 2007;298:42–51. <https://doi.org/10.1016/j.colsurfa.2006.12.056>.
- [55] Dukhin SS. Dynamic adsorption layer of a bubble with small Reynolds number. *Colloid J USSR* 1982;44(5):791.
- [56] Dukhin SS, Kovalchuk VI, Gochev GG, Lotfi M, Krzan M, Malysa K, et al. Dynamics of rear stagnant cap formation at the surface of spherical bubbles rising in surfactant solutions at large Reynolds numbers under conditions of small Marangoni number and slow sorption kinetics. *Adv Colloid Interf Sci* 2015;222: 260–74. <https://doi.org/10.1016/j.cis.2014.10.002>.
- [57] Ybert C, Di Meglio JM. Ascending air bubbles in protein solutions. *Eur Phys J B* 1998;4:313–9. <https://doi.org/10.1007/S100510050385/METRICS>.
- [58] Pawliszak P, Ulaganathan V, Bradshaw-Hajek BH, Manica R, Beattie DA, Krasowska M. Mobile or immobile? Rise velocity of air bubbles in high-purity water. *J Phys Chem C* 2019. <https://doi.org/10.1021/acs.jpcc.9b03526>.
- [59] Kosior D, Zawala J. Initial degree of detaching bubble adsorption coverage and the kinetics of dynamic adsorption layer formation. *Phys Chem Chem Phys* 2018; 20:2403–12. <https://doi.org/10.1039/c7cp06099h>.
- [60] Pawliszak P, Ulaganathan V, Bradshaw-Hajek BH, Miller R, Beattie DA, Krasowska M. Can small air bubbles probe very low frother concentration faster? *Soft Matter* 2021;17:9916–25. <https://doi.org/10.1039/D1SM01318A>.
- [61] Krzan M, Lunkenheimer K, Malysa K. On the influence of the surfactant's polar group on the local and terminal velocities of bubbles. *Colloids Surf A Physicochem Eng Asp* 2004;250:431–41. <https://doi.org/10.1016/j.colsurfa.2004.05.022>.
- [62] Ulaganathan V, Gochev G, Gehin-Delval C, Leser ME, Gunes DZ, Miller R. Effect of pH and electrolyte concentration on rising air bubbles in  $\beta$ -lactoglobulin solutions. *Colloids Surf A Physicochem Eng Asp* 2016;505:165–70. <https://doi.org/10.1016/j.colsurfa.2016.03.059>.
- [63] Zholkovskij EK, Koval'Chuk VI, Dukhin SS, Miller R. Dynamics of rear stagnant cap formation at low Reynolds numbers. 1. Slow sorption kinetics. *J Colloid Interface Sci* 2000;226:51–9. <https://doi.org/10.1006/jcis.2000.6786>.
- [64] Zhang B, Wang Z, Luo Y, Guo K, Zheng L, Liu C. A mathematical model for single CO<sub>2</sub> bubble motion with mass transfer and surfactant adsorption/desorption in stagnant surfactant solutions. *Sep Purif Technol* 2023;308:122888. <https://doi.org/10.1016/j.seppur.2022.122888>.
- [65] Frumkin AN, Levich VG. The effect of surface active substances on the motion at liquid interfaces. *Zh Fiz Khim* 1947;21:1183–204.
- [66] Lotfi M, Bastani D, Ulaganathan V, Miller R, Javadi A. Bubble in flow field: a new experimental protocol for investigating dynamic adsorption layers by using

- capillary pressure tensiometry. *Colloids Surf A Physicochem Eng Asp* 2014;460:369–76. <https://doi.org/10.1016/j.colsurfa.2013.11.011>.
- [67] Jasak H, Tuković Z. Automatic mesh motion for the unstructured finite volume method. *Trans Famena* 2006;30(2):1–20.
- [68] Tukovic Z, Jasak H. Simulation of free-rising bubble with soluble surfactant using moving mesh finite volume/area method. In: 6th International Conference on CFD in Oil & Gas, Metallurgical and Process Industries, Trondheim, Norway; 2008.
- [69] Pesci C, Weiner A, Marshall H, Bothe D. Computational analysis of single rising bubbles influenced by soluble surfactant. *J Fluid Mech* 2018;856:709–63. <https://doi.org/10.1017/jfm.2018.723>.
- [70] Wang J, Pang M, Lv F. Effect of adsorption dynamics on hydrodynamic characteristics of a bubble contaminated by surfactants at medium Reynolds numbers. *Microgravity Sci Technol* 2022;34:1–20. <https://doi.org/10.1007/S12217-022-09959-Y/FIGURES/18>.
- [71] <https://www.openfoam.com/>.
- [72] Clift R, Grace JR, Weber ME. *Bubbles, Drops, and Particles (Dover Civil and Mechanical Engineering)*. 1978. p. 380.
- [73] Vakarelski IU, Manica R, Li EQ, Basheva ES, Chan DYC, Thoroddsen ST. Coalescence dynamics of Mobile and immobile fluid interfaces. *Langmuir* 2018;34:2096–108. <https://doi.org/10.1021/ACS.LANGMUIR.7B04106>.
- [74] Moore DW. The velocity of rise of distorted gas bubbles in a liquid of small viscosity. *J Fluid Mech* 1965;23:749–66. <https://doi.org/10.1017/S0022112065001660>.
- [75] Loth E. Quasi-steady shape and drag of deformable bubbles and drops. *Int J Multiphase Flow* 2008;34:523–46. <https://doi.org/10.1016/J.IJMULTIPHASEFLOW.2007.08.010>.
- [76] Legendre D, Zemit R, Velez-Cordero JR. On the deformation of gas bubbles in liquids. *Phys Fluids* 2012;24:43303. <https://doi.org/10.1063/1.4705527/257602>.
- [77] Wegener M, Paul N, Kraume M. Fluid dynamics and mass transfer at single droplets in liquid/liquid systems. *Int J Heat Mass Transf* 2014;71:475–95. <https://doi.org/10.1016/j.ijheatmasstransfer.2013.12.024>.
- [78] Borkowski M, Zawala J. Influence of temperature on rising bubble dynamics in water and n-pentanol solutions. *Minerals* 2021;11. <https://doi.org/10.3390/min11101067>.
- [79] Ju E, Cai R, Sun H, Fan Y, Chen W, Sun J. Dynamic behavior of an ellipsoidal bubble contaminated by surfactant near a vertical wall. *Korean J Chem Eng* 2022;39:1165–81. <https://doi.org/10.1007/S11814-021-1035-6/METRICS>.
- [80] Zawala J, Swiech K, Malysa K. A simple physicochemical method for detection of organic contaminations in water. *Colloids Surf A Physicochem Eng Asp* 2007;302. <https://doi.org/10.1016/j.colsurfa.2007.02.047>.
- [81] Krzan M, Malysa K. Profiles of local velocities of bubbles in n-butanol, n-hexanol and n-nonanol solutions. *Colloids Surf A Physicochem Eng Asp* 2002;207:279–91. [https://doi.org/10.1016/S0927-7757\(02\)00163-2](https://doi.org/10.1016/S0927-7757(02)00163-2).
- [82] Loglio G, Degli Innocenti N, Tesei U, Cini R, Wang Q-S. Rising of gas bubbles in an aqueous medium in presence of surfactants. *Il Nuovo Cimento Della Soc Ital Fisica* 1989;12:289–304.
- [83] Reinhard Miller, Liggieri L. *Bubble and Drop Interfaces*. CRC Press; 2018.
- [84] Malysa K, Zawala J, Krzan M, Krasowska M. Bubbles rising in solutions; local and terminal velocities, shape variations and collisions with free surface. *Bubble Drop Interfaces* 2011;243–92. <https://doi.org/10.1163/EJ.9789004174955.1-558.91>.
- [85] Kowalczyk PB, Zawala J, Drzymala J. Concentration at the minimum bubble velocity (CMV) for various types of flotation frothers. *Minerals* 2017;7. <https://doi.org/10.3390/min7070118>.
- [86] Rabe M, Verdes D, Seeger S. Understanding protein adsorption phenomena at solid surfaces. *Adv Colloid Interf Sci* 2011;162:87–106. <https://doi.org/10.1016/J.CIS.2010.12.007>.
- [87] Lautenbach V, Hosseinpour S, Peukert W. Isoelectric point of proteins at hydrophobic interfaces. *Front Chem* 2021;9:712978. <https://doi.org/10.3389/FCHEM.2021.712978/BIBTEX>.
- [88] Mobius D, Miller R, editors. *Proteins at Liquid Interfaces*. Elsevier; 1998.
- [89] Lotfi M, Bahmani A, Bastani D. Hydrodynamics of rising air bubbles in mixture of proteins with non-ionic surfactants to declare their interaction at the air-water interface. *Sci Iran* 2022;29:3179–87. <https://doi.org/10.24200/SCI.2022.57989.5506>.
- [90] Dabestani M, Yeganehzad S, Krzan M, Miller R. Characterisation of egg white adsorption layers under equilibrium and dynamic conditions. *Colloids Surf A Physicochem Eng Asp* 2019;568:29–35. <https://doi.org/10.1016/J.COLSURFA.2019.01.066>.
- [91] Zawala J, Todorov R, Olszewska A, Exerowa D, Malysa K. Influence of pH of the BSA solutions on velocity of the rising bubbles and stability of the thin liquid films and foams. *Adsorption* 2010;16:423–35. <https://doi.org/10.1007/S10450-010-9232-3>.
- [92] Gawel D, Zawala J. Stability of liquid films formed by a single bubble and droplet at liquid/gas and liquid/liquid interfaces in bovine serum albumin solutions. *ACS Omega* 2021;6:18289–99. <https://doi.org/10.1021/acsomega.1c02188>.
- [93] Ulaganathan V, Krzan M, Lotfi M, Dukhin SS, Kovalchuk VI, Javadi A, et al. Influence of  $\beta$ -lactoglobulin and its surfactant mixtures on velocity of the rising bubbles. *Colloids Surf A Physicochem Eng Asp* 2014;460:361–8. <https://doi.org/10.1016/J.COLSURFA.2014.04.041>.
- [94] Zawala J, Niecikowska A. “bubble-on-demand” generator with precise adsorption time control. *Rev Sci Instrum* 2017;88. <https://doi.org/10.1063/1.5001846/962889>.
- [95] Kosior D, Wiertel-Pochopien A, Kowalczyk PB, Zawala J. Bubble formation and motion in liquids—a review. *Minerals* 2023;13. <https://doi.org/10.3390/min13091130>.
- [96] Kosior D, Zawala J, Todorov R, Exerowa D, Malysa K. Bubble bouncing and stability of liquid films formed under dynamic and static conditions from n-ctanol solutions. *Colloids Surf A Physicochem Eng Asp* 2014;460:391–400. <https://doi.org/10.1016/j.colsurfa.2013.11.022>.
- [97] Wiertel-Pochopien A, Zawala J. Rupture of wetting films formed by bubbles at a quartz surface in cationic surfactant solutions. *Chem Eng Technol* 2019;42:1371–80. <https://doi.org/10.1002/ceat.201900003>.
- [98] Wiertel-Pochopien A, Zawala J. Influence of dynamic adsorption layer formation on bubble attachment to quartz and mica surfaces in solutions of pure and mixed surface-active substances. *Physicochem Probl Miner Process* 2018;54:1083–94. <https://doi.org/10.5277/ppmp18129>.
- [99] Marsh RJ, Jones RAL, Sferrazza M, Penfold J. Neutron reflectivity study of the adsorption of  $\beta$ -Lactoglobulin at a hydrophilic solid/liquid Interface. *J Colloid Interface Sci* 1999;218:347–9. <https://doi.org/10.1006/JCIS.1999.6410>.
- [100] MacRitchie F. Reversibility of protein adsorption. *Stud Interf Sci* 1998;7:149–77. [https://doi.org/10.1016/S1383-7303\(98\)80051-3](https://doi.org/10.1016/S1383-7303(98)80051-3).
- [101] Svitova TF, Wetherbee MJ, Radke CJ. Dynamics of surfactant sorption at the air/water interface: continuous-flow tensiometry. *J Colloid Interface Sci* 2003;261:170–9. [https://doi.org/10.1016/S0021-9797\(02\)00241-2](https://doi.org/10.1016/S0021-9797(02)00241-2).
- [102] Fainerman VB, Miller R, Ferri JK, Watzke H, Leser ME, Michel M. Reversibility and irreversibility of adsorption of surfactants and proteins at liquid interfaces. *Adv Colloid Interf Sci* 2006;123–126:163–71. <https://doi.org/10.1016/J.CIS.2006.05.023>.
- [103] Jachimska B, Warszyński P, Malysa K. Effect of motion on lifetime of bubbles at n-butanol solution surface. *Colloids Surf A Physicochem Eng Asp* 1998;143:429–40. [https://doi.org/10.1016/S0927-7757\(98\)00382-3](https://doi.org/10.1016/S0927-7757(98)00382-3).
- [104] Jachimska B, Warszyński P, Malysa K. Effects of motion in n-hexanol solution on the lifetime of bubbles at the solution surface. *Progr Colloid Polym Sci* 2000;116:120–8.
- [105] Borkowski M, Kosior D, Zawala J. Effect of initial adsorption coverage and dynamic adsorption layer formation at bubble surface in stability of single foam films. *Colloids Surf A Physicochem Eng Asp* 2020:589. <https://doi.org/10.1016/j.colsurfa.2020.124446>.
- [106] Zawala J, Miguet J, Rastogi P, Atasi O, Borkowski M, Scheid B, et al. Coalescence of surface bubbles: the crucial role of motion-induced dynamic adsorption layer. *Adv Colloid Interf Sci* 2023;317. <https://doi.org/10.1016/j.cis.2023.102916>.
- [107] Niecikowska A, Zawala J, Malysa K. Influence of adsorption of n-alkyltrimethylammonium bromides (C<sub>8</sub>, C<sub>12</sub>, C<sub>16</sub>) and bubble motion on kinetics of bubble attachment to mica surface. *Physicochem Probl Miner Process* 2011;47.
- [108] Niecikowska A, Zawala J, Miller R, Malysa K. Dynamic adsorption layer formation and time of bubble attachment to a mica surface in solutions of cationic surfactants (C<sub>n</sub>TABr). *Colloids Surf A Physicochem Eng Asp* 2010:365. <https://doi.org/10.1016/j.colsurfa.2010.01.038>.
- [109] Lin G, Frostad JM, Fuller GG. Influence of interfacial elasticity on liquid entrapment in thin foam films. *Phys Rev Fluids* 2018;3. <https://doi.org/10.1103/PhysRevFluids.3.114001>.
- [110] Yampolskaya G, Platikanov D. Proteins at fluid interfaces: adsorption layers and thin liquid films. *Adv Colloid Interf Sci* 2006;128–130:159–83. <https://doi.org/10.1016/J.CIS.2006.11.018>.
- [111] Bhamla MS, Giacomini CE, Balemans C, Fuller GG. Influence of interfacial rheology on drainage from curved surfaces. *Soft Matter* 2014;10:6917–25. <https://doi.org/10.1039/c3sm52934g>.
- [112] Saad Bhamla M, Chai C, Alvarez-Valenzuela MA, Tajuelo J, Fuller GG. Interfacial mechanisms for stability of surfactant-laden films. *PLoS ONE* 2017;12. <https://doi.org/10.1371/journal.pone.0175753>.